Acta Neuropathologica
https://doi.org/10.1007/s00401-022-02535-z

ORIGINAL PAPER

# Histopathology of the cerebellar cortex in essential tremor and other neurodegenerative motor disorders: comparative analysis of 320 brains

**Elan D. Louis[1] · Regina T. Martuscello[2] · John T. Gionco[2] · Whitney G. Hartstone[2] · Jessica B. Musacchio[2] · Marisa Portenti[2] · Morgan McCreary[1] · Sheng-Han Kuo[3] · Jean-Paul G. Vonsattel[2,4] · Phyllis L. Faust[2]**

Received: 15 November 2022 / Revised: 14 December 2022 / Accepted: 22 December 2022
© The Author(s), under exclusive licence to Springer-Verlag GmbH Germany, part of Springer Nature 2023

## Abstract

In recent years, numerous morphologic changes have been identified in the essential tremor (ET) cerebellar cortex, distinguishing ET from control brains. These findings have not been fully contextualized within a broader degenerative disease spectrum, thus limiting their interpretability. Building off our prior study and now doubling the sample size, we conducted comparative analyses in a postmortem series of 320 brains on the severity and patterning of cerebellar cortex degenerative changes in ET ($n=100$), other neurodegenerative disorders of the cerebellum [spinocerebellar ataxias (SCAs, $n=47$, including 13 SCA3 and 34 SCA1, 2, 6, 7, 8, 14); Friedreich's ataxia (FA, $n=13$); multiple system atrophy (MSA), $n=29$], and other disorders that may involve the cerebellum [Parkinson's disease (PD), $n=62$; dystonia, $n=19$] versus controls ($n=50$). We generated data on 37 quantitative morphologic metrics, grouped into 8 broad categories: Purkinje cell (PC) loss, heterotopic PCs, PC dendritic changes, PC axonal changes (torpedoes), PC axonal changes (other than torpedoes), PC axonal changes (torpedo-associated), basket cell axonal hypertrophy, and climbing fiber-PC synaptic changes. Principal component analysis of z scored raw data across all diagnoses (11,651 data items) revealed that diagnostic groups were not uniform with respect to pathology. Dystonia and PD each differed from controls in only 4/37 and 5/37 metrics, respectively, whereas ET differed in 21, FA in 10, SCA3 in 10, MSA in 21, and SCA1/2/6/7/8/14 in 27. Pathological changes were generally on the milder end of the degenerative spectrum in ET, FA and SCA3, and on the more severe end of that spectrum in SCA1/2/6/7/8/14. Comparative analyses across morphologic categories demonstrated differences in relative expression, defining distinctive patterns of changes in these groups. In summary, we present a robust and reproducible method that identifies somewhat distinctive signatures of degenerative changes in the cerebellar cortex that mark each of these disorders.

**Keywords** Cerebellum · Dystonia · Essential tremor · Histopathology · Neurodegenerative · Spinocerebellar ataxia

## Introduction

Until recently, the pathological anatomy of essential tremor (ET) had been largely unexplored [26, 33], a fact that is surprising given the high prevalence of this disease [30]. ET is estimated to affect 7 million Americans (i.e., 2.2% of the entire US population) [31], with prevalence estimates exceeding 20% in advanced age [30]. For many years, the few postmortem studies that had been conducted were largely restricted to single case reports. In addition, qualitative rather than rigorous quantitative approaches were employed, many of the "ET" cases had other neurological disorders (e.g., chorea, dystonia) rather than ET, and studies had not enrolled control brains for contextual comparison [26, 33].

✉ Elan D. Louis
elan.louis@UTSouthwestern.edu

[1] Department of Neurology, University of Texas Southwestern, 5323 Harry Hines Blvd, Dallas, TX 75390-8813, USA

[2] Department of Pathology and Cell Biology, Columbia University Irving Medical Center and the New York Presbyterian Hospital, New York, NY, USA

[3] Department of Neurology, Vagelos College of Physicians and Surgeons, Columbia University, New York, NY, USA

[4] Taub Institute for Research on Alzheimer's Disease and the Aging Brain, Columbia University, New York, NY, USA

Published online: 06 January 2023

In recent years, we and others have identified a growing compendium of morphologic changes in the ET brain, predominantly centered in and around the Purkinje cells (PCs) in the cerebellar cortex [1, 2, 5–7, 18, 20, 22, 24, 27, 29, 36, 39, 46], and distinguishing ET from age-matched control brains. These changes were observed in the PC dendritic arbor and the PC axonal compartment as well as the connections between PCs and neighboring neuronal populations (climbing fibers, basket cells) [1, 2, 5–7, 18, 20, 24, 26, 27, 29, 36, 39, 46]. Several studies, from our group [1, 5, 7, 18–20, 22, 24, 27–29, 46] and others [36], also observed PC loss, along with increased distances between PC bodies and high percentages of empty baskets, both of which are indirect measures of PC loss.

The degree to which these same changes occur in other diseases, either those that are cerebellar degenerative [e.g., spinocerebellar ataxias (SCA), Friedreich's ataxia (FA), multiple system atrophy (MSA)] or those that are more broadly degenerative but physiologically also involving the cerebellum and manifesting tremor [e.g., Parkinson's disease (PD), dystonia], or are unique to ET is not clear. Thus, the above-mentioned findings [1, 2, 5–7, 18, 20, 24, 26, 27, 29, 36, 39, 46], which are based on ET-control comparisons, had not been put into a larger disease context. These changes had not been contextualized within a broader degenerative disease spectrum, and this limited their interpretability.

To address what was considered a gap in knowledge, we proposed a large comparative analysis with two phases (NIH R01 NS088257). Phase 1 (2015–2018) was a discovery phase–an initial sample of 156 brains including ET, 7 other diseases (dystonia, PD, SCA3, SCA1, SCA2, SCA6, MSA) and controls [26]. Phase 2 (2018–2022) was designed both as a validating phase—to double the total sample numbers as well as increase the number of disease states (now also including FA, SCA7, SCA8, SCA14). During each phase, data on a large number ($n = 37$) of quantitative morphologic metrics of cerebellar pathology were compared across these diseases.

Phase 1 suggested that that the degree of cerebellar degeneration in ET aligns it with a milder end in the spectrum of cerebellar degenerative disorders, and furthermore, that a somewhat distinctive signature of degenerative changes marks each of these disorders [26].

In this publication, we fully complete our analyses. We present data on 164 additional brains, thereby doubling our sample size; we further expand the number of disorders to include ET, 11 other diseases and controls; and we present the entire pooled data in its totality. As such, this represents not only the largest but the only organized effort to compare ET brains with brains of several other neurological disorders, for which such data are also surprisingly sparse. We present data on more than 300 brains and > 10,000 quantitative data points intensively collected over a 6-year period. Using this novel approach, which enables statistical comparisons based on composite analyses of multiple morphological metrics, we have now identified reproducible patterns of disease changes in cerebellar cortex across these numerous disorders. As such, these combined analyses (1) represent the most detailed and comprehensive analyses of ET neuropathology to date, (2) provide a direct connection between ET neuropathology and that which is observable in other degenerative motor disorders, and (3) present the results of a refined set of histopathological analyses of the cerebellar cortex in a family of disorders of cerebellar degeneration.

## Methods

### ET brain repository, study subjects and brains, and clinical assessment

Analyses included 320 brains in total. All study subjects signed informed consent forms approved by the respective university or institutional ethics boards.

All ET brains ($n = 100$) were from the Essential Tremor Centralized Brain Repository (ETCBR), a longstanding, joint collaboration between investigators at University Texas Southwestern Medical Center and Columbia Universities [26, 27]. Established in 2003, the ETCBR serves ET cases throughout the United States. ET diagnoses were carefully assigned by a senior movement disorders neurologist specializing in tremor (E.D.L.) who used three sequential methods, as documented in detail elsewhere [1, 26]. Briefly, the clinical diagnosis of ET was initially assigned by treating neurologists, and second, confirmed by E.D.L. who reviewed semi-structured clinical questionnaires, medical records and Archimedes spirals and who used the following criteria: (i) moderate or greater amplitude kinetic tremor (rating of 2 or higher [32]) in at least one of the submitted Archimedes spirals; (ii) no history of PD or dystonia; and (iii) no other etiology for tremor (e.g., medications, hyperthyroidism) [1, 26]. Third, a detailed, videotaped, neurological examination was performed, from which action tremor was rated and a total tremor score assigned [range 0–36 [maximum]) [1, 26]. This and clinical questionnaire data were used to assign a final diagnosis of ET [1, 26], using previously published diagnostic criteria [moderate or greater amplitude kinetic tremor (tremor rating ≥ 2) during three or more activities or a head tremor in the absence of PD or other known causes] [32], which have been shown to be both reliable and valid [25, 34]. None of the ET cases reported a history of traumatic brain injury, exposure to medications with associated cerebellar toxicity (e.g., phenytoin, chemotherapeutic agents), or heavy ethanol use, as defined [9]. Every 6–9 months, a follow-up semi-structured telephone evaluation was performed and hand-drawn spirals were

collected; a detailed, videotaped, neurological examination was repeated if there was concern about a new, emerging movement disorder. Many of the cases were also enrolled in a longitudinal, prospective study that necessitated regular, 18-month, detailed, videotaped neurological examinations (NIH R01 NS086736).

We were able to obtain 47 SCA brains (14 SCA1, 7 SCA2, 13 SCA3, 5 SCA6, 5 SCA7, 2 SCA8 and 1 SCA14) and 13 Friedreich's ataxia (FA) brains from multiple brain repositories: 34 from a hereditary ataxia specimen repository at the Veterans Affairs Medical Center in Albany, New York, 6 from the National Institutes of Health NeuroBioBank (University of Maryland, Baltimore, MD), 12 from the Center for NeuroGenetics Ataxia Brain Bank at the University of Florida, Gainesville FL, 7 from the University of Washington, Seattle WA, 1 from The Sheffield Biorepository at the University of Sheffield, Sheffield UK and 1 from the New York Brain Bank. As done previously [26], we grouped the SCA1, SCA2, SCA6, SCA7, SCA8, and SCA14 brains together (i.e., "SCA1/2/6/7/8/14", $n=34$) as these disorders are characterized by marked PC loss; by contrast, SCA3 ($n=13$) is not characterized by marked PC loss.

Tissue from 62 PD brains was obtained from the New York Brain Bank. We also obtained 29 MSA brains [16 from the New York Brain Bank, 2 from the University of Florida Neuromedicine Human Brain and Tissue Bank, Gainesville FL and 11 from the National Institutes of Health NeuroBioBank (3 from University of Miami, Miami, FL, 4 from University of Maryland, Baltimore, MD, and 4 from the Harvard Brain Tissue Resource Center, McLean Hospital, Belmont, MA)] and 19 dystonia brains [3 from the New York Brain Bank and 16 from the National Institutes of Health NeuroBioBank (8 from University of Maryland, and 8 from the Harvard Brain Tissue Resource Center, McLean Hospital, Belmont, MA)].

There were 50 control brains. Thirty-nine control brains were from the New York Brain Bank. These had been individuals who were prospectively followed at the Alzheimer's Disease Research Center or the Washington Heights Inwood Columbia Aging Project, Columbia University. During serial neurological examinations, these individuals were clinically free of ET and other neurodegenerative disorders, including Alzheimer's disease, PD, or progressive supranuclear palsy. Eleven control brains were obtained from the National Institutes of Health NeuroBioBank (eight from University of Miami, Miami, FL and three from University of Maryland, Baltimore, MD).

In sum, therefore, 320 postmortem brains were analyzed. Subject selection was guided by available tissue. We identified 100 ET cases from the New York Brain Bank and selected 50 controls to achieve a 2:1 ratio. We selected older controls whose ages most closely approximated those of our ET cases as well as a subset of younger controls ($n=18$, age 36–67 years), to provide some age-matching with other disease entities where death occurs at younger ages. These 100 ET cases had been selected to lack widespread marked hypoxic-ischemic damage, concurrent Alzheimer's-type changes that would meet criteria for high likelihood of Alzheimer's disease, or evidence of other neurodegenerative disease pathology such as progressive supranuclear palsy, corticobasal degeneration, Lewy body disease, or traumatic encephalopathy. We used all available SCA and dystonia brains from multiple sources and aimed to obtain approximately as many PD brains as controls. As presented in detail for our discovery dataset (Phase 1, $n=156$ brains) [26], we were adequately powered to detect cerebellar pathology across different diagnoses. By comparison, the combined dataset (Phases 1 and 2, $n=320$) now has double the number of brains for nearly all diagnostic categories (100 rather than 50 ET, 47 rather than 23 SCAs, 62 rather than 29 PD, 29 rather than 15 MSA, 50 rather than 25 controls) other than dystonia (19 rather than 14 dystonia).

## Tissue processing and initial neuropathologic examination

Brains from the New York Brain Bank had a complete neuropathological assessment with standardized measurements of brain weight (grams) and postmortem interval (hours between death and placement of brain in a cold room or upon ice) [1, 26]. Seventeen standardized blocks were harvested from each brain and processed, and 7 µm-thick formalin-fixed paraffin-embedded sections were stained with Luxol fast blue/hematoxylin and eosin (LH&E) [26, 35]. Additionally, selected sections were stained by the Bielschowsky method, and with mouse monoclonal antibodies to alpha-synuclein (clone KM51, Novocastra), phosphorylated tau (clone AT8, Research Diagnostics, Flanders, NJ) and beta-amyloid (clone 6F/3D, Dako, Carpenteria, CA) [26, 35]. All tissues were examined microscopically by a senior neuropathologist (J.P.G.V.) blinded to clinical information [26, 35]. Braak and Braak Alzheimer's disease staging for neurofibrillary tangles, Consortium to Establish a Registry for Alzheimer's disease (CERAD) ratings for neuritic plaques and Thal amyloid stage were assigned [3, 4, 26, 38]. Cerebellar tissues received from other brain repositories were from the same standard region as harvested at the New York Brain Bank. In most instances, brain weights (grams) were available, and in many instances, data were also available on postmortem interval, Braak Alzheimer's disease staging and CERAD staging.

## Quantification of PCs, torpedoes and additional cerebellar pathology

We obtained a standard $3\times20\times25$-mm formalin-fixed tissue block from each brain from a parasagittal slice located

1–1.5 cm from the cerebellar midline and containing anterior and posterior quadrangulate lobules and the underlying dentate nucleus [26]. We used this block to quantify 37 metrics, each of which was within one of the following eight broad categories of pathological change: (1) PC loss, (2) heterotopic PCs, (3) PC dendritic changes, (4) PC axonal changes (torpedoes), (5) PC axonal changes (other than torpedoes, e.g., recurrent collaterals, thickened axons), (6) PC axonal changes (torpedo-associated), (7) basket cell axonal hypertrophy, (8) climbing fiber-PC synaptic changes (Table 1 here and Fig. 1 in Louis et al. [26]). To account for variations in quantity of cerebellar cortex in the tissue block and/or microscopic field imaged, we normalized several of these metrics (i.e., we divided by the PC layer length) and expressed them as per mm [33], as described [26]. To account for PC loss, which may affect the ability to detect a PC-associated pathological change and thus result in an artificially low value [e.g., the counts for displaced PCs (i.e., heterotopic PCs) and the counts for normally placed PCs would be low when PCs are lost], we divided other metrics by the number of PCs [26]. We identified morphologic changes by a variety of methods, including histologic stains (LH&E, Bielschowsky), immunostain for calbindin$D_{28k}$ on 100 µm-thick vibratome sections [1, 26], dual immunostain for calbindin$_{28k}$ and glutamic acid decarboxylase (GAD) [19, 26], and immunostain for vesicular glutamate transporter type 2 (VGlut2) [15, 20, 26] (Table 1). For FA cases, 'wet' formalin fixed tissue to quantify metrics identified by calbindin$D_{28k}$ immunostain of 100 µm-thick tissue sections ($n = 21$ metrics, Table 1) was only available on four cases; the remaining 16 metrics that required only paraffin embedded tissue were performed on all 13 FA cases available. The composite of multiple metrics provided a comprehensive and mutually complementary view of pathological changes, which one metric alone would be unable to provide. Below we now describe each category of pathological change in detail.

#### PC cell loss

Metrics in this category include three measures of PC linear density, which differ with respect to the structures counted (e.g., PC cell bodies or PC nucleoli) and staining method (LH&E or calbindin$D_{28k}$ immunostain). "Empty baskets" were quantified by dual immunohistochemical staining for calbindin$D_{28k}$ and GAD in paraffin sections as the plexus of basket cell axons around the PC soma without a detectable PC body; the percentage of empty baskets provides an indirect measure of PC loss [19].

#### Heterotopic PCs

Heterotopic PCs are those whose cell body is misplaced in the molecular layer [27]. The metrics in this category include four measures of the number of heterotopic PCs, which differ with respect to the staining method (LH&E or calbindin$D_{28k}$ immunostain) and whether they were normalized to PC layer length or to the number of PCs.

#### PC dendritic changes

Focal swellings of PC dendritic processes, defined as rounded-to-ovoid masses in the molecular layer that are associated with PC dendrites [46] were quantified with six metrics. The six metrics differ with respect to the staining method (LH&E, Bielschowsky, or calbindin$D_{28k}$ immunostain) and whether they were normalized to PC layer length or to the number of PCs.

#### PC axonal changes (torpedoes)

Common among the axonal changes in ET are torpedoes, which are round or ovoid swellings of the proximal portion of the PC axon. In this category are seven metrics that differ with respect to the staining method used (in order of increasing sensitivity: LH&E, Bielschowsky, calbindin$D_{28k}$ immunostain), whether they were normalized to PC layer length or to the number of PCs, and whether axons with single torpedoes or axons with multiple torpedoes were counted.

#### PC axonal changes other than torpedoes

A variety of additional changes in PC axonal anatomy have been described in ET, including PC axonal recurrent collaterals, PC thickened axonal profiles, and PC axonal branching [1]. Other metrics were the PC plexus percentage (the percent of the length of the PC layer covered by a visible recurrent collateral plexus) [1] and PC puncta (the number of PCs with several dark puncta along the PC soma and proximal dendrites; it is proposed to represent the synapses of PC recurrent collaterals or aggregates of degenerating PC cytoplasm) [26]. PC terminal axonal sprouting (the presence of a frayed terminal axonal region) was rated using a 0–3 scale, as previously described [26]. In this category, the seven metrics all are based on calbindin$D_{28k}$ immunostains of 100 µm-thick cerebellar sections.

#### PC axonal changes (torpedo-associated)

In ET, PCs with torpedoes are more likely to have additional axonal changes (e.g., thickened profiles, recurrent collaterals, branching) than PCs without torpedoes [26]. The six metrics in this group assess axonal changes in PCs with torpedoes; the metrics are normalized either to the number of torpedoes (%) or the PC layer length (per mm). These metrics all are based in calbindin$D_{28k}$ immunostains of 100 µm-thick cerebellar sections.

**Table 1** Category of pathological changes and metrics

| Category of pathological change | Stain used | Metric | Published methods | Comment |
|---|---|---|---|---|
| PC cell loss | LH&E | PC body linear density (cells/mm) | See [5] | Adjusted for PC layer length |
| | LH&E | PC nucleolus linear density (cells/mm) | See [5] | Adjusted for PC layer length |
| | CB | PC body linear density (cells/mm) | See [22] | Adjusted for PC layer length |
| | CB-GAD | Percentage of empty baskets | See [19] | Indirect measure of PC loss |
| Heterotopic PCs | LH&E | Heterotopic PC linear density (cells/mm) | See [27] | Adjusted for PC layer length |
| | LH&E | Heterotopic PCs per PC | See [27] | Adjusted for the number of PCs |
| | CB | Heterotopic PC linear density (cells/mm) | See [27] | Adjusted for PC layer length |
| | CB | Heterotopic PCs per PC | See [27] | Adjusted for the number of PCs |
| PC dendritic changes | LH&E | PC dendritic swelling density (swellings/mm] | See [46] | Adjusted for PC layer length |
| | LH&E | PC dendritic swellings per PC | See [46] | Adjusted for the number of PCs |
| | Bielschowsky | PC dendritic swelling density (swellings/mm] | See [46] | Adjusts for PC layer length |
| | Bielschowsky | PC dendritic swellings per PC | See [46] | Adjusted for the number of PCs |
| | CB | PC dendritic swelling density (swellings/mm] | See [1] | Adjusted for PC layer length |
| | CB | PC dendritic swellings per PC | See [1] | Adjusted for the number of PCs |
| PC axonal changes (Torpedoes) | LH&E | Torpedo linear density (torpedoes/mm) | See [24] | Adjusted for PC layer length |
| | LH&E | Torpedoes per PC | See [24] | Adjusted for the number of PCs |
| | Bielschowsky | Torpedo linear density (torpedoes/mm) | See [35] | Adjusted for PC layer length |
| | Bielschowsky | Torpedoes per PC | See [35] | Adjusted for the number of PCs |
| | CB | Torpedo linear density (torpedoes/mm) | See [1] | Adjusted for PC layer length |
| | CB | Torpedoes per PC | See [1] | Adjusted for the number of PCs |
| | CB | Multiple ($\geq 2$) torpedo density (multiple torpedoes/mm) | See [1] | Adjusted for PC layer length |
| PC axonal changes (other than torpedoes) | CB | PC axonal recurrent collaterals density (recurrent collaterals per mm) | See [1] | Adjusted for PC layer length |
| | CB | PC thickened axonal profiles (thickened axonal profiles per mm) | See [1] | Adjusted for PC layer length |
| | CB | PC axonal branching (branches per mm) | See [1] | Adjusted for PC layer length |
| | CB | PC terminal sprout rating | See [26] | |
| | CB | PC plexus percentage | See [1] | |
| | CB | PC puncta density (puncta per mm) | See [26] | Adjusted for PC layer length |
| | CB | PC puncta per PC | See [26] | Adjusted for the number of PCs |
| PC axonal changes (torpedo-associated) | CB | Percentage of torpedoes with axonal recurrent collaterals | See [1] | |
| | CB | Torpedoes with axonal recurrent collaterals (per mm) | See [1] | Adjusted for PC layer length |
| | CB | Percentage of torpedoes with thickened axons | See [1] | |
| | CB | Torpedoes with thickened axons (per mm) | See [1] | Adjusted for PC layer length |
| | CB | Percentage of torpedoes with branching axons | See [1] | |
| | CB | Torpedoes with branching axons (per mm) | See [1] | Adjusted for PC layer length |
| Basket cell axonal hypertrophy | Bielschowsky | Basket cell rating | See [1] | |
| climbing fiber-PC synaptic changes | VGlut2 | Climbing fiber synaptic density | See [20] | |
| | VGlut2 | Percentage of climbing fibers in the outer 20% of the molecular layer | See [20] | |

*CB* calbindin, *GAD* glutamic acid decarboxylase, *LH&E* Luxol fast blue/hematoxylin and eosin, *PC* Purkinje cell, *VGLut2* vesicular glutamate transporter type 2

#### Basket cell axonal hypertrophy

This category includes a single metric—a semi-quantitative rating of the density of the basket cell axonal plexus surrounding PC bodies in Bielschowsky stain, with a scale of 0–3 [7]. This density is increased in ET, and likely reflects a secondary response to PC loss [7].

#### Climbing fiber-PC synaptic changes

This category includes two metrics assessing the distribution of climbing fiber-PC synapses on PC dendrites. One is a measure of the density of these synapses and the other is a measure of the re-distribution of these synapses to the parallel fiber synaptic territory in the outer 20% of the molecular layer [20].

### Statistical analyses

#### Comparing demographic and primary pathological features across diagnostic categories

We compared clinical and pathological features of each diagnostic group, using controls as our reference group. Categorical or ordinal variables were compared using Chi-square tests. For continuous variables, we tested for normality using the Kolmogorov–Smirnov test. If they were normally distributed, we compared continuous variables using Student's *t* tests; if they were not, we used Mann–Whitney tests.

#### Correlation between demographic and primary pathological features and quantitative morphologic metrics

We assessed whether postmortem features were associated with demographic or primary pathological features (e.g., postmortem interval). To avoid performing an excessive number of comparisons (i.e., there were 37 postmortem features), we selected one metric from each of the eight categories of pathological features. These eight core metrics were as follows; (1) The inverse of the PC body count per mm (LH&E stain), (2) heterotopic PCs per PC (LH&E stain), (3) PC dendritic swellings per mm (LH&E stain), (4) torpedoes per mm (Bielschowsky stain), (5) Purkinje cell terminal sprout rating (calbindin$D_{28k}$ immunostain), (6) torpedoes with recurrent collaterals per mm (calbindin$D_{28k}$ immunostain), (7) rating of basket cell axonal hypertrophy (Bielschowsky stain, mean value), (8) percentage of climbing fiber-Purkinje cell synapses in outer 20% of molecular layer (VGlut2 immunostain) [26].

We then assessed whether the eight core metrics correlated with age, sex, brain weight, Thal stage, Braak Alzheimer's disease staging, CERAD and postmortem interval. These analyses were performed separately in each of the following eight diagnostic categories: control, dystonia, PD, ET, SCA3, FA, MSA, and SCA1/2/6/7/8/14. Due to the large number of comparisons (8 core metrics × 7 variables × 8 diagnostic categories = 448), we used a Bonferroni correction to set the significant $p$ value at < 0.000112 (i.e., 0.05/448).

#### Principal component analysis

Due to the large number of metrics ($n = 37$), we first performed a principal component analysis to obtain a broad overview of the distribution of the data points and to identify underlying unifying dimensions (i.e., groupings of metrics). For this analysis, we used z-scored raw data for each metric across all diagnostic categories. We used the *PCA* function in GraphPad Prism v9.4 package to compute the principal components of the z-scored data, and the loadings function (coordinates of the variables divided by the square root of the eigenvalue associated with the component) to determine the correlation and weighted effect that each metric contributes to each principal component.

#### Quantifying change in each metric in each diagnosis

Next, for each diagnosis, we quantified the change in each metric, using controls as our reference group. To compute an average fold-change effect size for each metric in each diagnosis, we first calculated the average value of the control samples for each metric and the average value of each diagnosis' samples for each metric. Then, for each metric and diagnosis, we computed the $\log_2$-ratio of these two average values. We evaluated the statistical significance of these changes relative to controls using the Mann–Whitney test and corrected the resulting $p$ values for false discovery using the Benjamini–Hochberg method. There were differences in age between several diagnoses and controls. Therefore, we wanted to consider the effects of age on our data. To do so, we adjusted for age in a series of multiple linear regression models. Therefore, for each diagnosis, there were 37 models, with the dependent variable = metric data, and independent variables = diagnosis (disease vs. control) and age. We then compared the effect sizes in these adjusted models with those in our unadjusted analyses, using Spearman's rho [26].

#### Determining whether there is a core signature of cerebellar degeneration

To formally determine whether there was a robust co-varying core signature of cerebellar degeneration, the correlation

between all pairwise combinations of metrics was computed and the correlation coefficients were hierarchically clustered [26].

#### Examining patterns of change across diagnoses

We also generated three violin plots: (1) a "Severity Score" containing the core set of 25 highly correlated metrics, (2) a "PC Loss Score" [PC body/mm, percentage empty baskets], and (3) percentage of climbing fibers in the outer 20% of the molecular layer.

Finally, to further delineate the disease pattern in ET versus other primary disorders of cerebellar degeneration (SCA 3, SCA 1/2/6/7/8/14), we compared data from our eight core metrics to visually display group differences in a skyline plot. For this plot, we normalized our data so that each of the eight core metrics would appear to be on the same scale; otherwise some bars would have been several orders of magnitude greater than other bars and the plot would have been difficult to read. We normalized to one (i.e., the mean of each of the eight metrics was determined as well as the value that the mean would need to be multiplied by to be 1.0. For example, if the mean = 0.25, then that value would be 4.0. Then each data point in each brain was multiplied by this value. This operation was performed separately for each of the eight metrics) [26].

#### Developing a neuropathological scoring system

We developed a cumulative score derived from the morphologically most evident and biologically most relevant metrics. This comprised 10 metrics, as indicated by asterisks in Table 3 (although the inverse of LH&E PC/mm was used). For ET, controls and each of the remaining diagnoses, we reported the median, mean, 25th quartile and 75th quartile score for this "ET neuropathological score."

## Results

### Demographic and primary pathological features across diagnostic categories

Several of the groups differed from controls with respect to age, sex, brain weight, Thal stage, Braak stage, CERAD score and postmortem interval (Table 2). Several of these differences were expected given the natural history of these disorders, with younger ages of onset in FA, SCAs and MSA than in ET or PD.

### Correlation between demographic and primary pathological features and quantitative morphologic metrics

We generated data on 37 quantitative morphologic metrics that were further grouped into eight broad categories. As described in our statistical analysis section, we selected one metric from each of the eight categories and assessed whether these eight core metrics were correlated with age, sex, brain weight, Braak Alzheimer's disease staging, CERAD and postmortem interval. This operation was repeated in eight diagnostic categories. Given the large number of comparisons ($n = 448$), we set the significant $p$ value at $< 0.000112$. Only two correlations had p values that were $< 0.001$ and only one had a $p$ value that was less than 0.000112. These correlation analyses indicate that differences between diagnostic groups in these variables (e.g., age, sex, brain weight, Thal stage, etc.) were not likely to account for differences in cerebellar pathology between diagnostic groups; that is, they were not likely to be acting as confounders.

### Principal component analysis

Given the large number of metrics and data generated (37 metrics in nearly all of the 320 brains = 11,651 data items), we first performed principal component analysis of the z-scored raw data to identify underlying unifying dimensions (i.e., groupings of metrics). When analyzed across all diagnostic categories, the two major axes of variation in the data segregated individual patients into distinct groupings (Fig. 1a). To a large extent, the first axis of variation (principal component 1, PC1) separated MSA and SCA1/2/6/7/8/14 from the remaining diagnoses, with the data points in MSA and SCA1/2/6/7/8/14 distinctly situated to the right of the main cluster. The second axis of variation (principal component 2, PC2) mainly separated MSA from SCA1/2/6/7/8/14, with most data points for SCA1/2/6/7/8/14 located above those of MSA (Fig. 1a).

To the best of our knowledge, clinical intake diagnosis as MSA-parkinsonism (MSA-P) or MSA-cerebellar (MSA-C) subtypes [40] was available for 17 of 29 of MSA cases (16 from NYBB) and revealed differential stratification across the PCA graph. All 5 MSA cases with PC1 > 5 and PC2 > 0 that clustered on the upper right side of the PCA graph among SCA1/2/6/7/8/14 cases were MSA-C subtype (Fig. 1a), suggesting that with severe, typically near end-stage cerebellar involvement in MSA at autopsy, the metrics in this study do not distinguish them from also severely affected SCA cases; indeed, these entities have been broadly classified as olivopontocerebellar atrophies [12]. MSA-P cases ($n = 11$ with clinical diagnoses) were distributed in two regions of the PCA graph: (1) seven cases scattered

**Table 2** Demographic and pathological features by diagnosis

| | Control | Dystonia | PD | ET | Friedreich's ataxia | SCA3 | SCA 1/2/6/7/8/14 | MSA |
|---|---|---|---|---|---|---|---|---|
| N | 50 | 19 | 62 | 100 | 13 | 13 | 34 | 29 |
| Age at death (years) | 75.3 ± 16.1 [79.0] | 80.6 ± 8.8 [81] | 77.9 ± 6.3 [79.0] | 88.8 ± 6.1 [89.5] | 41.4 ± 18.1 [37.0] | 57.0 ± 11.3 [57.0] | 60.5 ± 16.1 [63.0] | 66.6 ± 9.0 [69.0] |
| | | $p = 0.09$ | $p = 0.25$ | $\mathbf{p = 0.001}$ | $\mathbf{p < 0.001}$ | $\mathbf{p = 0.001}$ | $\mathbf{p = 0.001}$ | $\mathbf{p = 0.003}$ |
| Male sex | 29 (58.0) | 4 (21.1) | 49 (79.0) | 36 (36.0) | 5 (38.5) | 7 (53.8) | 20 (58.8) | 11 (37.9) |
| | | $\mathbf{p = 0.006}$ | $\mathbf{p = 0.01}$ | $\mathbf{p = 0.01}$ | $p = 0.21$ | $p = 0.78$ | $p = 0.94$ | $p = 0.08$ |
| Brain weight (g) | 1.262 ± 184 | 1.272 ± 90 | 1.345 ± 137 | 1.188 ± 132 | 1.211 ± 132 | 1.186 ± 221 | 1.213 ± 204 | 1.222 ± 107 |
| | | $p = 0.87$ | $p = 0.06$ | $\mathbf{p = 0.02}$ | $p = 0.19$ | $p = 0.24$ | $p = 0.34$ | $p = 0.58$ |
| Median (range) Thal stage for beta-amyloid | 0 (0–2) | 1.5 (0–2) | 2 (0–3) | 1.5 (0–2) | NA | NA | 0 (0–3) | 0 (0–2) |
| | | $p = 0.15$ | $\mathbf{p = 0.001}$ | $\mathbf{p = 0.01}$ | | | $p = 0.33$ | $p = 0.96$ |
| Median (range) Braak Alzheimer's disease staging | 2 (0–5) | 1.5 (0–2) | 2 (0–4) | 3 (1–5) | NA | NA | 1 (0–4) | 1.5 (0–5) |
| | | $p = 0.36$ | $p = 0.82$ | $\mathbf{p = 0.001}$ | | | $p = 0.20$ | $p = 0.37$ |
| Median (range) CERAD | 0 (0–2) | 0 (0) | 1 (0–2) | 1 (0–3) | NA | NA | 0 (0–3) | 1 (0–3) |
| | | $p = 0.39$ | $\mathbf{p = 0.02}$ | $\mathbf{p = 0.02}$ | | | $p = 0.36$ | $p = 0.15$ |
| Median postmortem interval (h) | 5.8 | 25 | 1.8 | 2.2 | 28.5 | 12.0 | 6.7 | 16.8 |
| | | $\mathbf{p = 0.03}$ | $\mathbf{p = 0.001}$ | $\mathbf{p = 0.001}$ | $\mathbf{p = 0.01}$ | $p = 0.66$ | $\mathbf{p = 0.02}$ | $p = 0.12$ |

Values are mean ± standard deviation [median] or count (percentage) unless otherwise specified. Statistical comparisons are with controls

Bolded values are statistically significant ($p < 0.05$)

Categorical or ordinal variables were compared using Chi-squares. For continuous variable, we tested for normality using Kolmogorov–Smirnov test. If normally distributed, the variables were compared using the Student's *t* test. If not normally distributed, we compared groups using the Mann–Whitney test (non-parametric)

*CERAD* Consortium to Establish a Registry for Alzheimer's disease, *ET* essential tremor, *g* grams, *h* hours, *MSA* multiple system atrophy, *NA* not available, *PD* Parkinson's disease, *SCA* spinocerebellar ataxia

among other diagnoses on the left side of the PCA graph, although still with distinctly higher PC1 X-axis values than in controls (Fig. 1b, PC1 < 2); neuropathological examination showed predominant striatonigral degeneration, consistent with lesser cerebellar involvement in MSA-P, [12] and (2) four cases with PC1 > 5 and PC2 < 0, which had mixed striatonigral and cerebellar degeneration on neuropathological examination, suggesting a distinctive cerebellar pathology when MSA progresses to involve cerebellum versus that in most SCAs.

Figure 1c displays the strength of correlations between each metric and each principal component, with metrics that are a greater distance from the center (0.0, 0.0) contributing more to the principal components. The figure also shows the directionality of the relationship, reflecting their positive or negative contribution to each principal component. Each of the eight broad categories of metric is color-coded. The colors display clustering (e.g., green metrics lie close to other green metrics; yellow metrics lie close to other yellow metrics), a product of their membership in the same broad category; however, for many metrics the overlap is not complete, indicating that individual metrics within a category provide unique information. Several of the purple metrics are anti-correlated, which is expected given that the % empty baskets reflect PC loss whereas the others directly reflect PC counts. Metrics that are most strongly positively correlated with PC1 drive the separation of SCA1/2/6/7/8/14 and MSA from other diagnoses, including torpedo counts (green metrics), a subset of torpedo-associated changes in PC axons (blue metrics on right side) and PC dendritic swellings (yellow metrics). In contrast, metrics that were anti-correlated with PC1 reflect greater PC loss (purple metrics) and poorly preserved climbing fiber synapses (light blue metrics), which are features of SCA1/2/6/7/8/14 and MSA [17, 26]. Metrics that in Fig. 1a differentially correlate with PC2 and separate SCA1/2/6/7/8/14 and MSA, such as

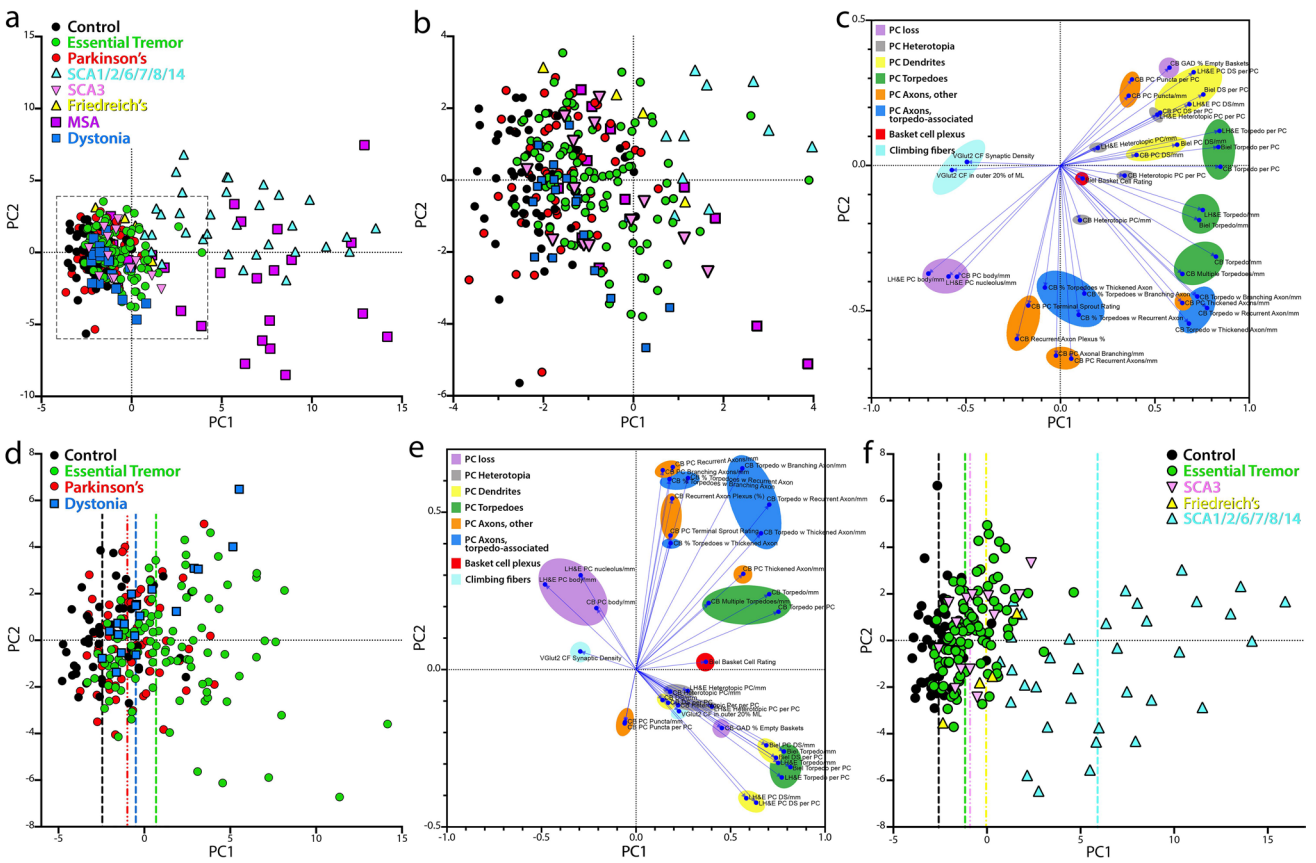


**Fig. 1** Principal component analyses of cerebellar morphologic metrics across diagnoses. Principal component analysis of the z-scored raw data across all eight diagnostic categories (**a**) or across select diagnoses **d**, **f** shows how individual patients distribute across the two major axes of variation in the data, identifying distinct disease groupings. Each dot represents data from an individual patient. Panel **b** is an enlargement of the boxed area in panel (**a**). Color coded vertical lines **d**, **f** denote the median change along the x-axis in principal component 1 for the corresponding diagnostic category. The loading graphs **c**, **e** portray the strength and directionality of the correlation between each metric with each principal component, with metrics that are a greater distance from the center (0.0, 0.0) being most correlated with the principal components. Metrics are color coded based on the eight categories of morphologic metrics, as indicated in the legend including Purkinje cell loss (purple), Purkinje cell heterotopia (gray), Purkinje cell dendrites (yellow), Purkinje cell torpedoes (green), Purkinje cell axons, other (orange), Purkinje cell axons, torpedo associated (blue), Basket cell plexus (red) and climbing fibers (light blue). 1c includes all diagnoses and 1e is limited to controls, ET, PD and dystonia. *CB* = calbindin, *GAD* glutamic acid decarboxylase, *LH&E* Luxol fast blue/hematoxylin and eosin, *PC* Purkinje cell, *PC1* principal component 1, *PC2* principal component 2, *VGlut2* vesicular glutamate transporter type 2

greater number of PC dendritic swellings and CB PC puncta (yellow metrics, Fig. 1c) in SCA1/2/6/7/8/14 and greater number of torpedo-associated changes in PC axons (blue metrics, Fig. 1c), other changes in PC axons (most orange metrics, Fig. 1c), and a somewhat better preserved PC population in MSA (purple metrics, Fig. 1c).

While controls, ET, PD, dystonia and several other diagnoses (e.g., FA, SCA3) form a dense cluster (Fig. 1a), there is considerable variance in these diagnoses along the axis of PC1 (Fig. 1b). When MSA, FA and all SCAs are excluded from the analysis, there is no complete overlap between ET, PD and dystonia, and variable segregation is apparent predominantly along the axis of PC1 (Fig. 1d). The median of all controls (black dots) centers at PC1 = − 2.46. Compared to controls, PD (red dots, median PC1 = − 1.00) and dystonia (blue squares, median PC1 = − 0.51) patients are shifted slightly to the right in close proximity to one another. ET patients (green dots) are shifted even more considerably the right (median PC1 = 0.67).

Figure 1e limits its analysis to controls, ET, PD and dystonia, and portrays the strength of correlation between each metric and each principal component. Similar to that in Fig. 1c, the colors display clustering, a product of their membership in the same group; however, the overlap is not complete. Again, the two sets of purple metrics are anti-correlated, with expected inverse relationship between % empty baskets and PC counts. In this dataset, VGlut2 climbing fibers in outer 20% of the molecular layer and VGlut2 climbing fiber synaptic density (light blue metrics) show

opposite correlations with PC1, reflecting greater number of climbing fibers in outer 20% of the molecular layer (positive correlation) and lower VGlut2 climbing fiber synaptic density (negative correlation) as commonly seen in ET cases. Notably, the basket cell rating (red metric) has a stronger positive correlation with PC1 in this dataset (Fig. 1e) compared to that including all diagnoses (Fig. 1c), consistent with its enrichment in ET cerebellum vs. controls [7].

We also compared the principal component data for ET, FA, and all SCAs, as disorders whose primary identifiable pathology is most evident in the cerebellum, versus controls (Fig. 1f). The distribution of data for ET (green dots), SCA3 (pink triangles) and FA (yellow triangles) are shifted to the right versus controls (black dots) along the PC1 x-axis, with median values at − 2.58 (controls), − 1.17 (ET), − 0.91 (SCA3) and − 0.05 (FA). Notably, there is significant overlap in data points for SCA3 and FA and many ET cases. SCA1/2/6/7/8/14 patients (blue dots) are shifted to a much greater extent along both PC1 (median = 5.91) and PC2 axes, and some of those data points overlap with those of ET, FA and SCA3. In considering only FA and individual SCA disorders (Supplemental Fig. 1), the principal component data show similar median PC1 x-axis values for SCA3 (− 3.46, pink triangles) and FA (− 3.01, yellow triangles), consistent with an overall lower burden of cerebellar cortical pathology in these disorders, and increasing PC1 medians for SCA1 (0.51, green circles), SCA7 (1.10, blue triangles), SCA2 (2.13, orange circles) and SCA6 (4.81, purple circles). The most severe cerebellar pathology typically seen in SCA6 is consistent with the cerebellar cortex being the major focus of disease in this disorder [42].

In summary, these analyses showed that these diagnoses were not uniform with respect to cerebellar pathology, with the greatest (though not identical) changes observed in MSA and SCA1/2/6/7/8/14 and lesser changes in the other groups (Fig. 1a–e). In terms of primary disorders of cerebellar degeneration, among which changes were most evident, the changes lay along a spectrum, with those observed in ET, SCA3 and FA forming the mildest grouping and those in SCA1/2/6/7/8/14 being the most severe relative to controls (Fig. 1f). As a whole, these latter disorders are arrayed along a spectrum of cerebellar of degeneration.

## Quantifying change in each metric in each diagnosis

We next quantified the change in each metric for each diagnosis, using controls as our reference group (Fig. 2a). Metrics (rows) and diagnoses (columns) are shown. Each cell in the heatmap is the average $\log_2$-fold-change (disease vs. control) for each metric. Dark purple cells indicate that there is a high mean value for the metric relative to controls; green cells indicate the opposite. Elements labeled with an asterisk indicate that the difference from controls is statistically significant, with false discovery rate < 0.01. We can make several observations.

First, when compared to controls, dystonia differed significantly in only 4/37 metrics (see four asterisks in dystonia column). PD differed significantly from controls in only 5/37 metrics (see five asterisks in PD column). By contrast, the number of differing metrics was 21 for ET. For FA and SCA3, the numbers were less (10 in each disorder). The number was 21 for MSA and 27 for SCA1/2/6/7/8/14 (Fig. 2a).

Second, in 17 metrics across 6 categories [i.e., PC loss, heterotopic PCs, PC dendritic changes, PC axonal changes (torpedoes), PC axonal changes (other than torpedoes), and PC axonal changes (torpedo-associated)], there was a spectrum of change, with ET generally at the low end and SCA1/2/6/7/8/14 or MSA at the high end of severity (Fig. 2a, Table 3). Dystonia did not differ from controls in any of these metrics, and PD differed from controls in only 2/18 metrics (LH&E PC body/mm, CB PC thickened axons/mm).

Third, for three metrics, including the percentage climbing fibers in the outer 20% of the molecular layer (VGlut2) and two metrics involving PC puncta (calbindin$D_{28k}$), the pattern observed for ET was not merely on the cerebellar degeneration spectrum. The mean percentage of climbing fibers in the outer 20% of the molecular layer (VGlut2) was distinctly increased in ET compared to controls, whereas in SCA1/2/6/7/8/14 and MSA there was a decrease compared with controls (Fig. 2a, c). In addition, ET is the only diagnosis in which increased climbing fibers in outer 20% of the molecular layer is accompanied by significantly decreased climbing fiber synaptic density. Of interest, increased climbing fibers in outer 20% of molecular layer is also seen in FA, but this is not accompanied by a decrease in climbing fiber synaptic density, demonstrating a novel disease pattern. The density of PC puncta (calbindin$D_{28k}$) was only significantly increased in SCA1/2/6/7/8/14, and involved a larger percentage of PCs when seen in a sample. In all other disorders, these structures were rare.

As there were differences in age between several diagnoses and controls, we adjusted for the effects of age using a series of multiple linear regression models. We then compared the effect sizes in these adjusted models with those in our unadjusted analyses, using Spearman's rho. The effect sizes (i.e., fold-difference in each metric between each disease and control) were strikingly similar as were the direction of these differences, indicating that observed differences in the unadjusted analyses were nearly universally conserved in the age-adjusted analyses (Supplemental Fig. 2).

Finally, in our primary analyses we grouped SCA1/2/6/7/8/14 together. For a secondary analysis, we examined the spectrum of changes in each of the 37 metrics across SCA 1, 2, 6 and 7 subtypes [excluding SCA8

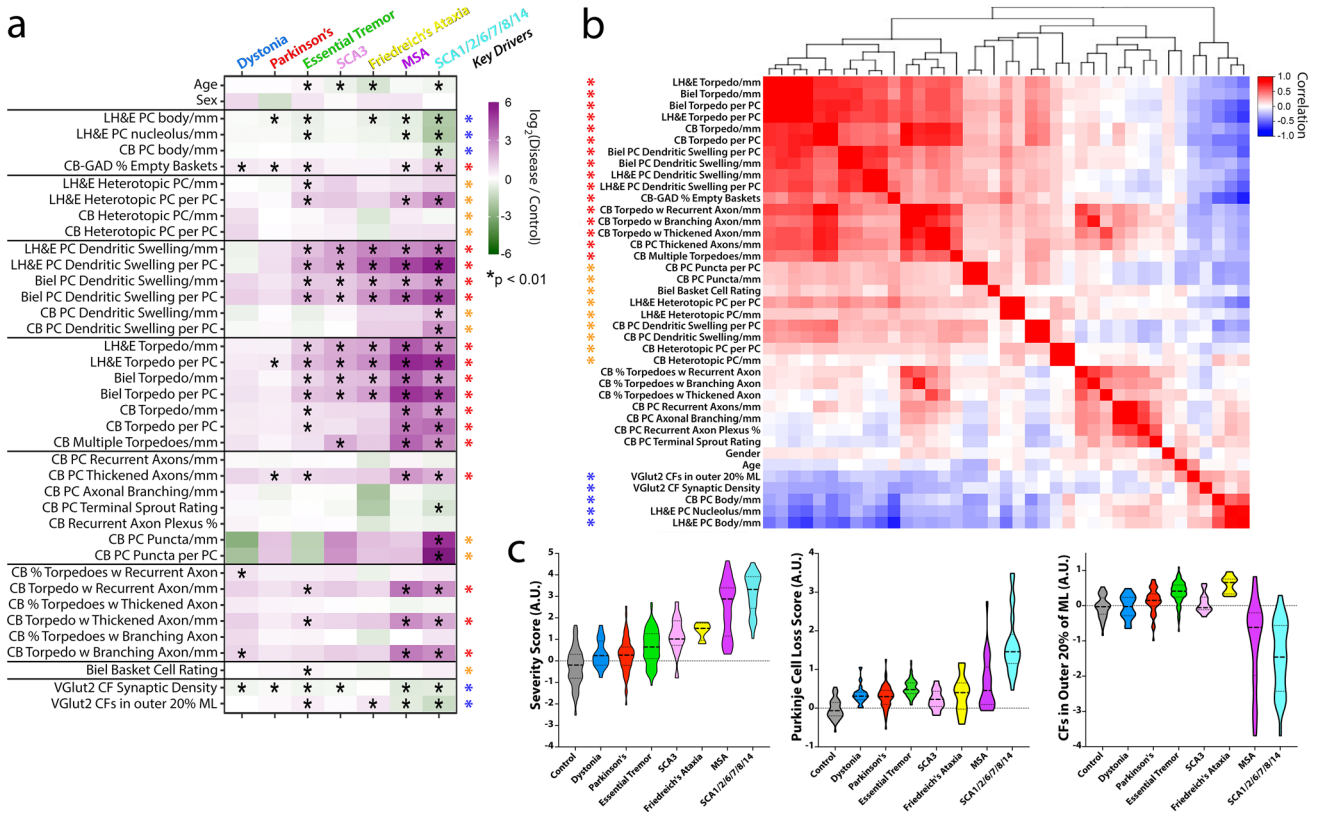


**Fig. 2** Differences in fold-change for each metric across diseases and key pathologic drivers. **a** Metrics (rows) and diagnoses (columns) are shown. Each cell in the heatmap is the average $\log_2$-fold-change (disease vs. control) for each metric. The scale ranges from dark purple (high relative to control) to dark green (low relative to control). Elements with a black asterisk indicate a statistically significant difference vs. controls (Mann–Whitney test, *p* values corrected for false discovery by Benjamini–Hochberg method; * = FDR < 0.01). **b** Hierarchical clustering of the correlation coefficients between all pairwise combinations of metrics, with colored scale of red (positive correlation), white (no correlation) and blue (negative correlation). Many of the prominent positively correlated (red and orange asterisks) or negatively correlated (blue asterisk) variables are the same variables that differ across disease categories (see black asterisks in **2a**), and are designated here as "*Key Drivers*" in (**a**). **c** Three scores were computed across disease categories by combining the average fold-change (disease/control) for selected metrics and plotted on a $\log_2$-transformed scale, including a "Severity Score" (large block of 25 positively correlated red and orange metrics in panel (**b**)), a "Purkinje Cell Loss Score" (inverse Purkinje cell body and percent empty baskets), and a score reflecting climbing fibers (CFs) in the outer 20% of the molecular layer. Within each violin, the dashed line shows the median value and the dotted lines indicate outer quartiles in the data distribution. Data for Friedreich's ataxia was derived from 4 cases in whom metrics from calbindin$D_{28k}$ staining was performed and 13 cases for all other metrics performed in paraffin sections

(*n* = 2) and SCA14 (*n* = 1) due to limited sample size] (Supplemental Fig. 3). Overall, the SCA subtypes were broadly similar in the direction of fold-change versus controls (i.e., purple and green colors indicate increased versus decreased, respectively) when samples were either grouped (Fig. 2a) or separated out (Supplemental Fig. 3). There were some differences in terms of the extent of fold-change between these SCAs, as demonstrated by the color saturation, indicating that these SCA subtypes, though broadly similar, are not identical.

## Determining whether there is a core signature of cerebellar degeneration

To formally determine whether there was a robust co-varying core signature of cerebellar degeneration, the correlation between all pairwise combinations of observables was computed and the correlation coefficients were hierarchically clustered (Fig. 2b). A large red block of observables (16 metrics) was all strongly positively correlated with each other and represent a core, common phenotypic signature mainly related to torpedoes, other axonal changes and dendritic swellings (red asterisks). Nine additional metrics were correlated with each other, although to a lesser degree (orange asterisks), and mainly relate to heterotopic PCs and PC swellings. Other metrics were anti-correlated (Fig. 2b,

**Table 3** Metrics in which a spectrum of pathological changes was observed

| Category of pathological change | Stain | Metric | Spectrum of change observed |
|---|---|---|---|
| PC cell loss | LH&E | PC body linear density (cells/mm)* | √ |
| | LH&E | PC nucleolus linear density (cells/mm) | √ |
| | CB | PC body linear density (cells/mm) | |
| | CB-GAD | Percentage of empty baskets* | |
| Heterotopic PCs | LH&E | Heterotopic PC linear density (cells/mm) | |
| | LH&E | Heterotopic PCs per PC* | √ |
| | CB | Heterotopic PC linear density (cells/mm) | |
| | CB | Heterotopic PCs per PC | |
| PC dendritic changes | LH&E | PC dendritic swelling linear density (swellings/mm) | √ |
| | LH&E | PC dendritic swellings per PC | √ |
| | Bielschowsky | PC dendritic swelling linear density (swellings/mm) | √ |
| | Bielschowsky | PC dendritic swellings per PC* | √ |
| | CB | PC dendritic swelling linear density (swellings/mm) | |
| | CB | PC dendritic swellings per PC | |
| PC axonal changes (Torpedoes) | LH&E | Torpedo linear density (torpedoes/mm) | √ |
| | LH&E | Torpedoes per PC* | √ |
| | Bielschowsky | Torpedo linear density (torpedoes/mm) | √ |
| | Bielschowsky | Torpedoes per PC | √ |
| | CB | Torpedo linear density (torpedoes/mm) | √ |
| | CB | Torpedoes per PC | √ |
| | CB | Multiple torpedo density (multiple torpedoes/mm) | √ |
| PC axonal changes (other than torpedoes) | CB | PC axonal recurrent collaterals density (recurrent collaterals per mm) | |
| | CB | PC thickened axonal profiles density (thickened axonal profiles per mm)* | √ |
| | CB | PC axonal branching density (branches per mm) | |
| | CB | PC terminal sprout rating | |
| | CB | PC plexus percentage | |
| | CB | PC puncta density (PC with puncta per mm) | |
| | CB | PC puncta per PC | |
| PC axonal changes (torpedo-related) | CB | Percentage of torpedoes with axonal recurrent collaterals | |
| | CB | Torpedoes with axonal recurrent collaterals (per mm)* | √ |
| | CB | Percentage of torpedoes with thickened axons | |
| | CB | Torpedoes with thickened axons (per mm) | √ |
| | CB | Percentage of torpedoes with branching axons | |
| | CB | Torpedoes with branching axons (per mm) | |
| Basket cell axonal hypertrophy | Bielschowsky | Basket cell rating* | |
| Climbing fiber-PC synaptic changes | VGlut2 | Climbing fiber synaptic density in molecular layer | |
| | VGlut2 | Percentage of climbing fibers in the outer 20% of the molecular layer* | |

√ = a spectrum of change was observed, with ET generally at the low end and SCA1/2/6/7/8/14 or MSA at the high end of severity

*CB* calbindin, *GAD* glutamic acid decarboxylase, *LH&E* Luxol fast blue/hematoxylin and eosin, *PC* Purkinje cell, *VGLut2* vesicular glutamate transporter type 2

*10 metrics in the ET neuropathological score

blue squares and asterisks), consistent with a common tendency to lose PCs and climbing fiber synapses in several cerebellar diseases. In sum, these co-varying morphologic metrics defined "Key Drivers" of cerebellar pathology, which correlated with many of the statistically significant differences across disease categories (Fig. 2a, red, orange and blue asterisks).

## Examining patterns of change across diagnoses

Next, we computed scores for each patient as a fold-change relative to control averaged over selected observables and plotted on a $\log_2$-transformed scale (Fig. 2c), including (1) a "Severity Score" containing the core set of 25 highly correlated observables (Fig. 2b, red and orange asterisks), (2) a "PC Loss Score" [inverse PC body/mm, percentage empty baskets] and (3) climbing fibers in the outer 20% of the molecular layer. The "Severity Score" varied across diagnoses, with median scores for dystonia and Parkinson's disease being closest to controls; ET, SCA3 and FA were in the middle; and MSA and SCA1/2/6/7/8/14 were furthest from controls. The median PC loss score was furthest from controls in SCA1/2/6/7/8/14, closest to controls in dystonia, PD, and SCA3, and intermediate in ET, FA and MSA (which had wide variability). The climbing fiber outer 20% score showed an increase in ET and FA. In sum, these data demonstrate that ET had both common and distinctive combinations of morphologic patterns across a spectrum of cerebellar degeneration.

PC axonal and dendritic disease pathologies across these categories are observed in calbindin$D_{28k}$ immunostained cerebellar sections, demonstrating varying degrees of changes in axonal shape (e.g., torpedoes, thickened axons) and connectivity (e.g., recurrent collaterals, axonal branching), PC body changes (PC loss, heterotopias) and PC dendritic swellings (Fig. 3). These PC changes are observed in cerebellar cortex of SCA3 and FA (Fig. 3b, c), but are more prominently seen in ET (Fig. 3d). SCA1/2/6/7/8/14 and MSA have a wide range of PC loss, along with often marked increases in PC axonal changes (Fig. 3e–h, n–p); there was near complete loss of PC cellular elements in one SCA8 case (Fig. 3i). PC changes are less marked, although still distinguished from controls, in individuals with MSA-striatonigral predominant degeneration (Fig. 3n, MSA-SND) (i.e., corresponding to MSA-P cases in principal component analysis that cluster among ET and controls, Fig. 1b), whereas in MSA predominated by cerebellar atrophy (MSA-OPCA), only few PCs may remain, although those surviving are still often associated with axonal torpedoes [Fig. 3p, corresponding to MSA-C cases that cluster in principal component analysis among SCA cases (Fig. 1a)]. With mixed striatonigral-olivopontocerebellar degeneration (SND-OPCA) in MSA, there was a distinctive pattern where there are numerous PC axonal torpedoes throughout cerebellar cortex and many are associated with prominent recurrent axons (Fig. 3o), a feature that may contribute to separation of these MSA cases from most SCA cases in principal component analysis (Fig. 1a, MSA cases in lower right quadrant). Foci where clusters of axonal torpedoes are associated with prominent recurrent axons are also seen in other diseases, including ET, SCA1, SCA2, SCA7 (Fig. 3j–m), SCA6 (Fig. 3g) and focally in FA (inset in Fig. 3c), suggesting a common process of PC axonal rerouting in cerebellar disease that would disconnect PCs from their target cerebellar nuclei and contribute to a reorganization of intracortical cerebellar circuitry.

In several disease entities the calbindin$D_{28k}$ immunostain also identified rare highly degenerate PCs with a halo-like arrangement of multiple dendrite processes emanating from the cell soma, including in ET, FA, SCA1, SCA2, SCA6, SCA8 and MSA (Fig. 4). These abnormal dendrites were often hyperspiny, and spines were also seen on the PC soma. In a subset of these cells, a residual PC dendrite still present in the molecular layer had marked regressive changes and/or dendrite swellings (Fig. 4a, b, d, e, white caret). These findings suggest an extreme degenerative phenotype in these PCs.

Last, to further delineate the disease pattern in ET versus primary disorders of cerebellar degeneration (SCAs), we compared data from our eight core metrics to show their deviation from the norm in a skyline plot (Fig. 5). For most metrics, SCA1/2/6/7/8/14 had higher values than ET and SCA3, although not for all. In ET, the redistribution of climbing fiber synapses to the outer 20% of the PC arbor is highest (light blue bars), whereas climbing fiber synapses are markedly destroyed in SCA1/2/6/7/8/14. The *patterns* of pathological changes observed in ET, SCA3 and SCA1/2/6/7/8/14 differed from one another, with the relative heights of the bars to one another varying both within and across diagnostic categories. Thus, it is apparent that ET, SCA3 and SCA1/2/6/7/8/14 differed with respect to the relative expression (i.e., signature) of the degenerative features.

## Developing a neuropathological scoring system

We developed a cumulative score derived from the morphologically most evident and biologically most relevant metrics, representing each category of pathological change. This comprised ten metrics, selected on the basis of their strength in differentiating disease diagnoses in the principal component analysis and control-disease fold change analyses (Figs. 1, 2a). Next to each of the ten metrics is an asterisk (Table 3; the inverse of LH&E PC/mm was used). For ET, controls and each of the remaining diagnoses, we reported the median, mean, 25th quartile and 75th quartile score for this ET neuropathological score (Supplemental Table 1). The mean score for ET was slightly higher than that for SCA3 and very similar to that of FA, approximately 50% higher than that of PD, approximately 25% higher than that of dystonia and double that of controls. It was markedly less than that of MSA and SCA1/2/6/7/8/14 (Supplemental Table 1). Furthermore, there was diagnostic separation between ETs and controls, with the score for the lower 25% quartile of ET cases (1.224) exceeding the upper 75% quartile of controls (1.211). Last, there was a

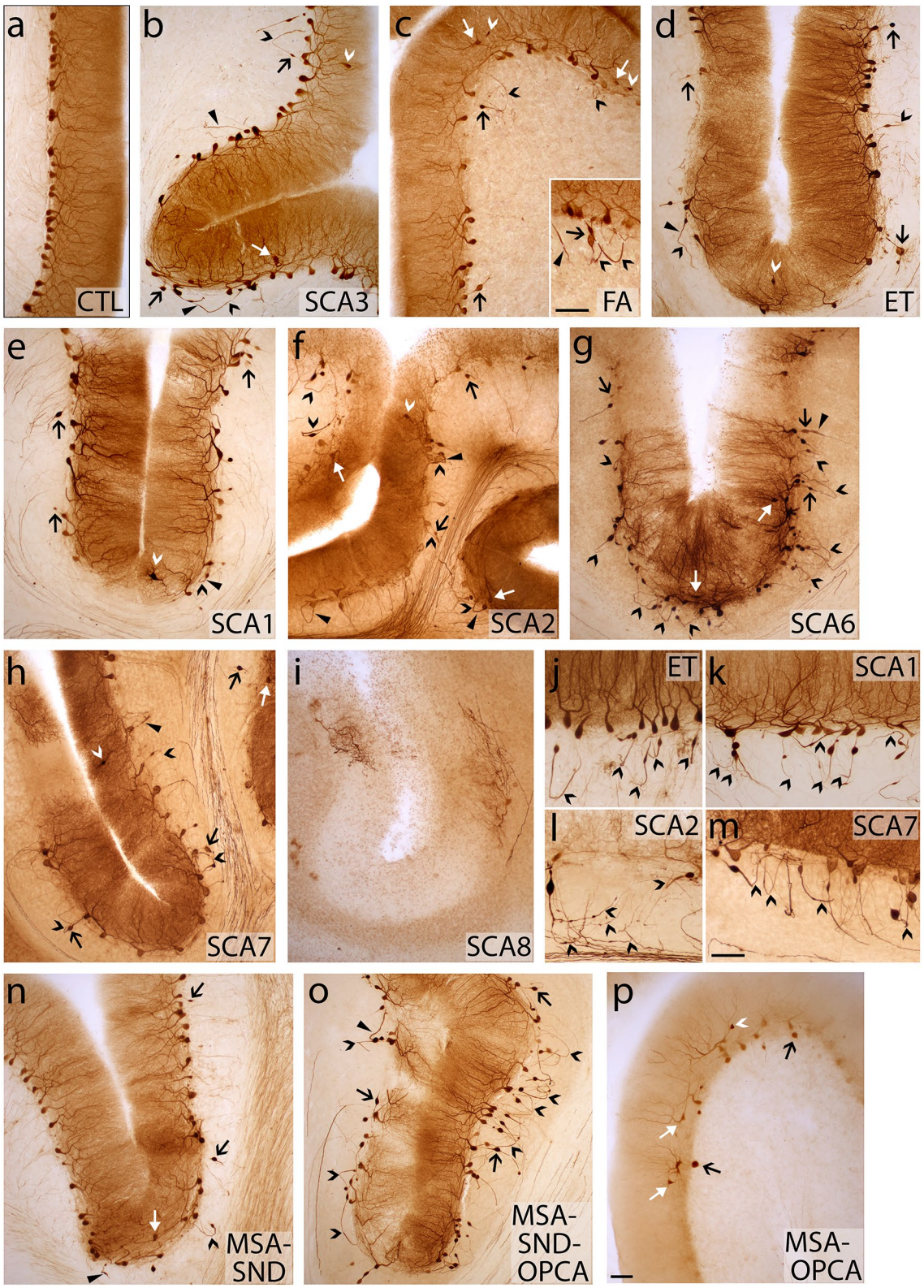
a
CTL
b
SCA3
c
FA
d
ET
e
SCA1
f
SCA2
g
SCA6
h
SCA7
i
SCA8
j
ET
k
SCA1
l
SCA2
m
SCA7
n
MSA-
SND
o
MSA-
SND-
OPCA
p
MSA-
OPCA

◂**Fig. 3** Calbindin$D_{28k}$ immunohistochemistry on 100-µm cerebellar neocortex sections across diagnoses. Several categories of morphologic changes in Purkinje cells are identified, including cell body loss, heterotopia (white arrow, **b**, **c**, **f**, **g**, **n**, **p**), dendrite swelling (white caret, **b–f**, **h**, **p**), and axonal changes including torpedoes (large black arrow, **b–h**, **n–p**), thickened axons (arrowhead, **b**, **c [inset]**, **d–h**, **n**, **o**) and recurrent collaterals on torpedo bearing axons (black caret, **h**, **j–o**). **a** Normal appearance of Purkinje cell dendrites and cell bodies and thin axon profiles in the granule cell layer of a control. **b**, **c** SCA3 and Friedreich's ataxia (FA) with intermediate axonal changes including torpedoes, thickened axons and recurrent collaterals. Heterotopic Purkinje cells and dendrite swellings are present. In FA, a focus with multiple torpedoes associated with recurrent collaterals is shown (inset, **c**). **d** Axonal changes and Purkinje cell loss are more prominent in essential tremor (ET). A dendrite swelling is present. **e–i** Spectrum of changes in SCA1/2/6/7/8 with moderate to severe Purkinje cell body and dendrite loss, abundant torpedoes, thickened axons and torpedo associated recurrent collaterals. **J–m** Foci in ET (**j**), SCA1 (**k**), SCA2 (**l**) and SCA7 (**m**) where there are clusters of torpedo bearing axons with recurrent collaterals. **n–o** Spectrum of change in MSA, being mild in cases with predominant striatonigral degeneration (MSA-SND, **n**) and severe in cases with predominant olivopontocerebellar atrophy (MSA-OPCA, **p**). In MSA with mixed striatonigral and olivopontocerebellar atrophy (MSA-SNA-OPCA, **o**), there are numerous torpedoes that predominantly have recurrent collaterals. *SCA* spinocerebellar ataxia, *MSA* multiple system atrophy. Scale bar, 100 µm in **m**, **p**, inset in **c**

marginal but not significant correlation between the ET scores and disease duration (Spearman's rho = 0.16, $p = 0.10$).

## Discussion

A growing compendium of morphologic changes has been identified in the ET brain, centered in the cerebellar cortex [1, 2, 5–7, 18, 20, 24, 27, 29, 36, 39, 46]. These findings, based exclusively on ET-control comparisons, had not been contextualized within a broader degenerative disease spectrum. To address this gap in knowledge, we conducted a two phase study in which data on a large number of quantitative morphologic metrics of cerebellar pathology were compared in ET, controls and several other diseases. Phase 1, based on 156 brains, suggested that that the degree of cerebellar degeneration in ET aligns it with a milder end in the spectrum of cerebellar degenerative disorders, and furthermore, that a somewhat distinctive signature of degenerative changes marks each of these disorders [26]. Phase 2 involved 164 additional brains, and we now present the entire pooled data in their totality. Many of our initial observations from Phase 1 are borne out again in Phase 2, thereby providing the needed construct validity for our first round findings. In addition, by increasing the number of disease comparators, several novel features are now identified.

From these pooled data, we make several core observations. First, although mild changes were observed in the cerebellum of dystonia and Parkinson's disease, these were nowhere near the magnitude or number observed in disorders whose primary identifiable pathology is most evident in the cerebellum (i.e., ET, SCA3, FA, SCA1/2/6/7/8/14 and MSA to varying degrees) (Figs. 1a, 2a). Second, within the latter group of diseases, there was a marked spectrum of change, with ET, SCA3 and FA generally near the lower end and SCA1/2/6/7/8/14 and MSA at the high end of severity (Figs. 1f, 2a, c). Thus, the degenerative changes observed in ET lie on the milder end of what is observed in disorders of cerebellar degeneration. In large part, the changes observed across ET and the other disorders of cerebellar degeneration comprised differences of *degree* rather than *kind*, likely reflecting a stereotypic repertoire of cellular reactions that characterize cerebellar degeneration. Third, several features distinctive to specific disorders were also identified, including a redistribution of climbing fiber synapses to the outer PC dendritic arbor in ET and FA and aggregation of calbindin$D_{28k}$-positive puncta around the PC soma most prominently in SCA1/2/6/7/8/14 (Fig. 2a). FA was the only disorder in which there was redistribution of climbing fiber synapses in the molecular layer but preserved climbing fiber synaptic density. Each of these disorders had a different signature with respect to cerebellar degeneration, as evidenced by our metric "scores" that combine categories of morphologic features (Fig. 2c) and a skyline plot (Fig. 5), which showed that different patterns emerged for ET, SCA3 and SCA1/2/6/7/8/14, indicating that these disorders of cerebellar degeneration do not form a homogeneous entity. In this sense, there were differences not only of *degree*, but also of *kind*.

As noted in our Phase 1 study [26], the constellation of pathological changes in the PC and neighboring neuronal populations in ET are not occurring in isolation with respect to one another; rather, they are likely operating as part of a system, as suggested by the array of morphologic changes that formed core "Key Drivers" of cerebellar pathology (Fig. 2a, b). The "Key Drivers" delineated in our prior study were identified again in this expanded sample set, and the strength of some additional correlations increased, such as enrichment of high basket cell rating in ET samples (Fig. 2a) [7].

As reviewed elsewhere, some of the cerebellar cortical changes are likely to be primary, whereas others are likely to be responsive, secondary and reparative [23]. The morphologic metrics we analyzed highlight the variability in mechanisms underlying cerebellar cortical degeneration. For instance, in both SCA3 and FA, the brunt of degeneration in cerebellum is centered in the dentate nucleus [13], and it has been traditionally viewed that the cerebellar cortex is relatively normal in these disorders. The findings in this study demonstrate that the cerebellar cortex is not normal in SCA3 or FA, yet their patterns of degeneration differ from each other and from ET. In SCA3 there was relative preservation of PCs, and secondary changes seen in ET such as basket

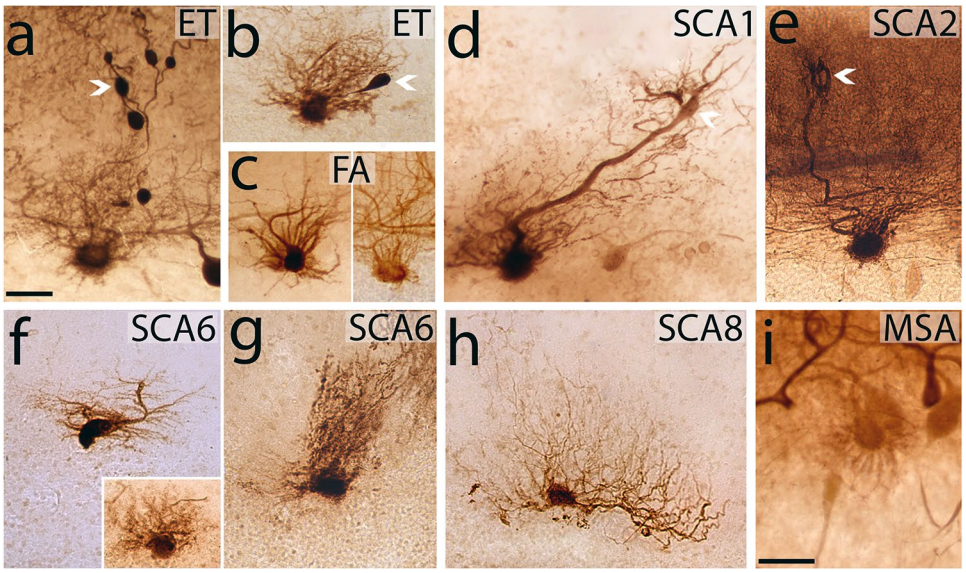


**Fig. 4** Dendritic and spine abnormalities in highly degenerate Purkinje cells. Calbindin$D_{28k}$ immunohistochemistry on 100-µm cerebellar neocortex sections in essential tremor (ET, **a**, **b**), Friedreich's ataxia (FA, **c**), SCA1 (**d**), SCA2 (**e**), SCA6 (**f**, **g**), SCA8 (**h**) and MSA (**i**) identifies Purkinje cells with a halo-like arrangement of multiple thin dendrites from the Purkinje cell soma and somatic spines. Dendrite swellings are associated with residual dendrites from these cells in the molecular layer (white caret, **a**, **b**, **d**, **e**). *SCA* spinocerebellar ataxia, *MSA* multiple system atrophy. Scale bars (in **a**, **i**), 50 µm

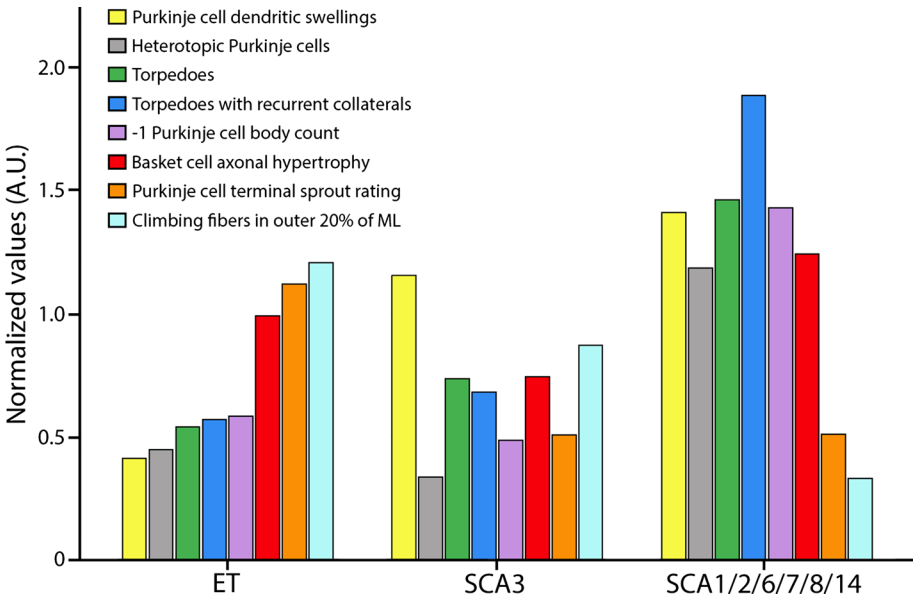


**Fig. 5** Skyline Plot—Patterns of degenerative changes across disorders. The median value for each of our eight core metrics are graphed in essential tremor (ET) cases in comparison to primary disorders of cerebellar degeneration (i.e., SCAs), including the following: basket cell axonal hypertrophy rating scale (red bar, Bielschowsky stain), heterotopic Purkinje cells per Purkinje cell (gray bar, LH&E stain), PC terminal sprout rating (orange bar, calbindin$D_{28k}$ immunostain), torpedoes per Purkinje cell (green bar, LH&E stain), torpedoes with recurrent collaterals/mm (blue bar, calbindin$D_{28k}$ immunostain), Purkinje cell dendritic swellings per Purkinje cell (yellow bar, Bielschowsky stain), inverse (-1) Purkinje cell body/mm (purple bar, LH&E stain), Climbing fibers in outer 20% of ML (light blue bar, VGlut2 immunostain). *ET* essential tremor, *ML* molecular layer, *SCA* spinocerebellar ataxia

cell axonal hypertrophy, heterotopic un-anchoring of PCs and climbing fiber redistribution to the outer PC dendritic arbor in the setting of PCs loss are less apparent in SCA3 [26], but significantly increased PC dendrite swellings and torpedoes were still detected and climbing fiber abnormalities were limited to milder decreases in synaptic density. In FA, PC loss was widely variant but overall median change was like that in ET (although occurring at a much younger patient age), there were increased PC axonal torpedoes and dendrite swellings, and a unique pattern of climbing fiber changes with increased climbing fiber extension to the outer PC dendritic arbor but preserved climbing fiber synaptic density. The common occurrence of increased PC dendritic swellings and torpedoes seen in both SCA3 and FA may reflect a dying-back-type PC degeneration due to loss of PC terminals in cerebellar nuclei, although direct effects on the

PC are not excluded. The decreased climbing fiber synaptic density in SCA3 may reflect combinations of mild PC dendrite changes and/or brainstem degeneration that may include mild neuronal loss in the inferior olive [42]. Redistribution of climbing fiber synapses to the outer 20% of the PC arbor correlates with degenerative regressive changes in the PC dendritic arbor in ET, which have been demonstrated in detail with Golgi staining in ET [29], and similarly reflected by our finding of increased PC dendritic swellings in FA along with a prior pathological study demonstrating abnormal PC arbors in one FA case [14]. Inferior olive degeneration is not characteristically seen in either FA [16] or ET [21]; while this may explain preservation of climbing fiber synaptic density in FA, the exact mechanisms of this synaptic loss in ET remains to be fully discerned, although loss of PC dendritic spines may lead to climbing fiber synaptic loss in ET [29].

In more severe forms of cerebellar degeneration (e.g., in SCA1/2/6/7/8/14, MSA), nearly all cerebellar pathologies are seen, commensurate with a greater degree of PC damage, but climbing fiber changes are dominated by regression of synapses in the molecular layer, potentially associated with both marked PC loss and/or degenerative changes in the inferior olive [17]. Furthermore, our studies in MSA identified a somewhat distinctive pattern of PC axonal pathology, with widespread presence of numerous PC axons bearing torpedoes associated with prominent recurrent collaterals when MSA initially involves the cerebellar cortex. Nonetheless, foci with similar clusters of torpedoes associated with recurrent collaterals were seen in ET and several SCAs. We previously demonstrated that axonal recurrent collaterals were threefold more frequently seen on the axons of PCs with torpedoes versus Purkinje cells without torpedoes in ET [1]. In sum, these findings suggest a common process of rerouting of torpedo-bearing PC axonal connections away from cerebellar nuclei that contributes to the reorganization of intracortical cerebellar circuitry in several cerebellar degenerative diseases.

We also observed a halo-like sprouting of multiple fine dendritic processes from the PC soma and somatic spines in rare PCs in ET, FA, SCA1, SCA2, SCA6 SCA8 and MSA (Fig. 4). PCs normally have somal spines and a multidendritic morphology during their early development [37]. Thus, the marked regression seen in these PCs associated with disease may reflect disturbance to the normal highly polarized PC morphology and resulting plasticity changes that recapitulate processes occurring in normal development. PCs with similar morphology have been described in several neurodegenerative diseases, including inherited ataxias [11, 41, 44, 45]; in one study it was shown that these somal spiny dendrites in PCs form local synaptic connections [10]. In SCA31, this multidendendritic morphology was associated with fragmentation of the Golgi apparatus [45], and other studies have shown that mislocalization of the Golgi apparatus leads to multidendritic morphology in PCs [8, 43].

During Phase 1, we developed an "ET neuropathological score", which in the future might be of value for diagnostic purposes, although further studies are needed to test and validate these as possible criteria [26]. The results from Phase 2 were replicative of those in Phase 1. That is, the value for ET was like that for SCA3, markedly higher than that for PD or dystonia, yet also markedly less than that for MSA and SCA1/2/6/7/8/14 (Supplemental Table 1). Furthermore, there was diagnostic separation between ETs and controls, with the score for the lower 25% quartile of ET cases (1.224) exceeding the upper 75% quartile of controls (1.211).

This study should be interpreted within the context of certain limitations. (1) There was some heterogeneity in the age at death of our disease groups. However, in correlational analyses, we showed that age was not correlated with our metrics of pathological change, indicating that age differences were not likely to account for differences in cerebellar pathology between groups. (2) We restricted our sampling to one region in the cerebellar hemisphere involved in motor function, and it would be of considerable interest in future studies to sample additional cerebellar regions. (3) Additional studies of the dentate nucleus, a site of major pathology in patients with SCA3 and FA, of cerebellar white matter in which different compartments (e.g., amiculum, album) may degenerate according to variable involvement of cerebellar afferents, and of other pathologies (e.g., glial pathologies including microgliosis), would further add to the neuroanatomical understanding of and ability to derive distinctions between these various diseases of the cerebellum [26]. (4) Cerebellar cortical atrophy, which has been reported in some neurodegenerative disorders, could paradoxically result in higher PC linear densities, thereby masking PC loss. We did not collect data on cerebellar weight, so we could not adjust for such potential atrophy. However, one of our metrics of PC loss was based on a dual immunostain for calbindin$_{28k}$ and GAD. This metric was expressed as a percentage rather than a linear density and, therefore, was not sensitive to atrophy. Our data showed that SCA1/2/6/7/8/14 cases demonstrated significant increases in the percentage of empty baskets (Fig. 2a). The study had numerous strengths including the following: (1) the large number of brains overall, (2) inclusion of not only ET and control brains, but also numerous other neurodegenerative disorders characterized by cerebellar involvement and/or tremor, (3) the ability to compare ET to several forms of SCA, including those in which PC loss is a feature and others in which it is not, (4) the detailed assessment of numerous metrics of cerebellar pathology in the SCAs and FA, as such studies are rare. Potentially, this combined quantitative morphologic method could be applied to other brain regions outside of cerebellum

and in other neurodegenerative diseases to identify patterns of pathological processes in neurologic disorders.

In summary, the degree of degeneration that is observed in ET brains aligns it with numerous other disorders of cerebellar degeneration. These changes in ET are on the milder end of what is observed in that spectrum. There is some evidence that all these disorders do not blandly express the same generic pattern of degeneration, with their only distinguishing feature being the degree to which they express that pattern, and that a somewhat distinctive signature of degenerative changes marks each of these disorders.

**Supplementary Information** The online version contains supplementary material available at https://doi.org/10.1007/s00401-022-02535-z.

**Acknowledgements** Brain tissue was derived from: New York Brain Bank at Columbia University; Dr. Arnulf H. Koeppen, Veterans Affairs Medical Center, Albany, New York, USA; the National Institutes of Health NeuroBioBank (University of Maryland, Baltimore, MD, University of Miami, Miami, FL, and Harvard Brain Tissue Resource Center, McLean Hospital, Belmont, MA); Dr. Laura Ranum, Center for NeuroGenetics Ataxia Brain Bank at the University of Florida, Gainesville FL; Dr. Todd Goldie, University of Florida Neuromedicine Human Brain and Tissue Bank, Gainesville FL; Dr. C. Dirk Keene, University of Washington, Seattle WA; and The Sheffield Biorepository at the University of Sheffield, Sheffield UK. We would like to thank all the patients and families that contributed to brain donation and the National Ataxia Foundation for providing funding to investigators for banking of brains from individuals with ataxia.

**Author contributions** All authors contributed to the study conception and design. Material preparation, data collection and analysis were performed by EDL, RTM, JTG, WGH, JBM, MP, MM, S-HK, J-PGV, and PLF. The first draft of the manuscript was written by EDL and all authors commented on previous versions of the manuscript. All authors read and approved the final manuscript.

**Funding** This work was supported by NINDS R01 NS088257 and NINDS R01 NS117745 (Drs. Louis and Faust, PIs) and R01 NS086736 (Dr. Louis, PI), which provide funding for the Essential Tremor Centralized Brain Repository.

**Data availability** Basic, anonymized demographic, clinical and tissue data are available as Supplemental Online material.

## Declarations

**Conflict of interest** None of the authors report any competing or financial interests.

**Ethical approval** All study subjects signed informed consent forms approved by the respective university or institutional ethics boards.

## References

1. Babij R, Lee M, Cortes E, Vonsattel JP, Faust PL, Louis ED (2013) Purkinje cell axonal anatomy: quantifying morphometric changes in essential tremor versus control brains. Brain 136:3051–3061. https://doi.org/10.1093/brain/awt238
2. Beliveau E, Tremblay C, Aubry-Lafontaine E, Paris-Robidas S, Delay C, Robinson C et al (2015) Accumulation of amyloid-beta in the cerebellar cortex of essential tremor patients. Neurobiol Dis 82:397–408. https://doi.org/10.1016/j.nbd.2015.07.016
3. Braak H, Alafuzoff I, Arzberger T, Kretzschmar H, Del Tredici K (2006) Staging of Alzheimer disease-associated neurofibrillary pathology using paraffin sections and immunocytochemistry. Acta Neuropathol 112:389–404. https://doi.org/10.1007/s00401-006-0127-z
4. Braak H, Braak E (1997) Diagnostic criteria for neuropathologic assessment of Alzheimer's disease. Neurobiol Aging 18:S85-88
5. Choe M, Cortes E, Vonsattel JG, Kuo SH, Faust PL, Louis ED (2016) Purkinje cell loss in essential tremor: random sampling quantification and nearest neighbor analysis. Mov Disord 31:393–401. https://doi.org/10.1002/mds.26490
6. Delay C, Tremblay C, Brochu E, Paris-Robidas S, Emond V, Rajput AH et al (2014) Increased LINGO1 in the cerebellum of essential tremor patients. Mov Disord 29:1637–1647. https://doi.org/10.1002/mds.25819
7. Erickson-Davis CR, Faust PL, Vonsattel JP, Gupta S, Honig LS, Louis ED (2010) "Hairy baskets" associated with degenerative Purkinje cell changes in essential tremor. J Neuropathol Exp Neurol 69:262–271. https://doi.org/10.1097/NEN.0b013e3181d1ad04
8. Fujishima K, Kurisu J, Yamada M, Kengaku M (2020) βIII spectrin controls the planarity of Purkinje cell dendrites by modulating perpendicular axon-dendrite interactions. Development 147:dev194530. https://doi.org/10.1242/dev.194530
9. Harasymiw JW, Bean P (2001) Identification of heavy drinkers by using the early detection of alcohol consumption score. Alcohol Clin Exp Res 25:228–235. https://doi.org/10.1111/j.1530-0277.2001.tb02203.x
10. Hirano A, Llena JF, French JH, Ghatak NR (1977) Fine structure of the cerebellar cortex in Menkes Kinky-hair disease. X-chromosome-linked copper malabsorption. Arch Neurol 34:52–56. https://doi.org/10.1001/archneur.1977.00500130072014
11. Ito H, Kawakami H, Wate R, Matsumoto S, Imai T, Hirano A et al (2006) Clinicopathologic investigation of a family with expanded SCA8 CTA/CTG repeats. Neurology 67:1479–1481. https://doi.org/10.1212/01.wnl.0000240256.13633.7b
12. Iwabuchi K, Koyano S, Yagishita S (2022) Simple and clear differentiation of spinocerebellar degenerations: overview of macroscopic and low-power view findings. Neuropathology 42:379–393. https://doi.org/10.1111/neup.12823
13. Koeppen AH (2018) The neuropathology of the adult cerebellum. Handb Clin Neurol 154:129–149. https://doi.org/10.1016/B978-0-444-63956-1.00008-4
14. Koeppen AH (1991) The Purkinje cell and its afferents in human hereditary ataxia. J Neuropathol Exp Neurol 50:505–514. https://doi.org/10.1097/00005072-199107000-00010
15. Koeppen AH, Davis AN, Morral JA (2011) The cerebellar component of Friedreich's ataxia. Acta Neuropathol 122:323–330. https://doi.org/10.1007/s00401-011-0844-9
16. Koeppen AH, Mazurkiewicz JE (2013) Friedreich ataxia: neuropathology revised. J Neuropathol Exp Neurol 72:78–90. https://doi.org/10.1097/NEN.0b013e31827e5762
17. Kuo SH, Lin CY, Wang J, Sims PA, Pan MK, Liou JY et al (2017) Climbing fiber-Purkinje cell synaptic pathology in tremor and cerebellar degenerative diseases. Acta Neuropathol 133:121–138. https://doi.org/10.1007/s00401-016-1626-1
18. Kuo SH, Tang G, Louis ED, Ma K, Babji R, Balatbat M et al (2013) Lingo-1 expression is increased in essential tremor cerebellum and is present in the basket cell pinceau. Acta Neuropathol 125:879–889. https://doi.org/10.1007/s00401-013-1108-7
19. Lee PJ, Kerridge CA, Chatterjee D, Koeppen AH, Faust PL, Louis ED (2019) A quantitative study of empty baskets in essential

tremor and other motor neurodegenerative diseases. J Neuropathol Exp Neurol 78:113–122. https://doi.org/10.1093/jnen/nly114
20. Lin CY, Louis ED, Faust PL, Koeppen AH, Vonsattel JP, Kuo SH (2014) Abnormal climbing fibre-Purkinje cell synaptic connections in the essential tremor cerebellum. Brain 137:3149–3159. https://doi.org/10.1093/brain/awu281
21. Louis ED, Babij R, Cortes E, Vonsattel JP, Faust PL (2013) The inferior olivary nucleus: a postmortem study of essential tremor cases versus controls. Mov Disord 28:779–786. https://doi.org/10.1002/mds.25400
22. Louis ED, Babij R, Lee M, Cortes E, Vonsattel JP (2013) Quantification of cerebellar hemispheric purkinje cell linear density: 32 ET cases versus 16 controls. Mov Disord 28:1854–1859. https://doi.org/10.1002/mds.25629
23. Louis ED, Faust PL (2020) Essential tremor pathology: neurodegeneration and reorganization of neuronal connections. Nat Rev Neurol 16:69–83. https://doi.org/10.1038/s41582-019-0302-1
24. Louis ED, Faust PL, Vonsattel JP, Honig LS, Rajput A, Pahwa R et al (2009) Torpedoes in Parkinson's disease, Alzheimer's disease, essential tremor, and control brains. Mov Disord 24:1600–1605. https://doi.org/10.1002/mds.22567
25. Louis ED, Ford B, Bismuth B (1998) Reliability between two observers using a protocol for diagnosing essential tremor. Mov Disord 13:287–293. https://doi.org/10.1002/mds.870130215
26. Louis ED, Kerridge CA, Chatterjee D, Martuscello RT, Diaz DT, Koeppen AH et al (2019) Contextualizing the pathology in the essential tremor cerebellar cortex: a patholog-omics approach. Acta Neuropathol 138:859–876. https://doi.org/10.1007/s00401-019-02043-7
27. Louis ED, Kuo SH, Tate WJ, Kelly GC, Gutierrez J, Cortes EP et al (2018) Heterotopic Purkinje cells: a comparative postmortem study of essential tremor and spinocerebellar ataxias 1, 2, 3, and 6. Cerebellum 17:104–110. https://doi.org/10.1007/s12311-017-0876-3
28. Louis ED, Kuo SH, Vonsattel JP, Faust PL (2014) Torpedo formation and Purkinje cell loss: modeling their relationship in cerebellar disease. Cerebellum 13:433–439. https://doi.org/10.1007/s12311-014-0556-5
29. Louis ED, Lee M, Babij R, Ma K, Cortes E, Vonsattel JP et al (2014) Reduced Purkinje cell dendritic arborization and loss of dendritic spines in essential tremor. Brain 137:3142–3148. https://doi.org/10.1093/brain/awu314
30. Louis ED, McCreary M (2021) How common is essential tremor? Update on the worldwide prevalence of essential tremor. Tremor Other Hyperkinet Mov (NY) 11:28. https://doi.org/10.5334/tohm.632
31. Louis ED, Ottman R (2014) How many people in the USA have essential tremor? Deriving a population estimate based on epidemiological data. Tremor Other Hyperkinet Mov (NY) 4:259. https://doi.org/10.7916/D8TT4P4B
32. Louis ED, Ottman R, Ford B, Pullman S, Martinez M, Fahn S et al (1997) The Washington heights-inwood genetic study of essential tremor: methodologic issues in essential-tremor research. Neuroepidemiology 16:124–133. https://doi.org/10.1159/000109681
33. Louis ED, Vonsattel JP, Honig LS, Ross GW, Lyons KE, Pahwa R (2006) Neuropathologic findings in essential tremor. Neurology 66:1756–1759. https://doi.org/10.1212/01.wnl.0000218162.80315.b9
34. Louis ED, Wendt KJ, Albert SM, Pullman SL, Yu Q, Andrews H (1999) Validity of a performance-based test of function in essential tremor. Arch Neurol 56:841–846. https://doi.org/10.1001/archneur.56.7.841
35. Louis ED, Zheng W, Mao X, Shungu DC (2007) Blood harmane is correlated with cerebellar metabolism in essential tremor: a pilot study. Neurology 69:515–520. https://doi.org/10.1212/01.wnl.0000266663.27398.9f
36. Mavroudis I, Kazis D, Petridis F, Chatzikonstantinou S, Karantali E, Njau SN et al (2022) Morphological and morphometric changes in the Purkinje cells of patients with essential tremor. Exp Ther Med 23:167. https://doi.org/10.3892/etm.2021.11090
37. McKay BE, Turner RW (2005) Physiological and morphological development of the rat cerebellar Purkinje cell. J Physiol 567:829–850. https://doi.org/10.1113/jphysiol.2005.089383
38. Mirra SS (1997) The CERAD neuropathology protocol and consensus recommendations for the postmortem diagnosis of Alzheimer's disease: a commentary. Neurobiol Aging 18:S91-94. https://doi.org/10.1016/S0197-4580(97)00058-4
39. Paris-Robidas S, Brochu E, Sintes M, Emond V, Bousquet M, Vandal M et al (2012) Defective dentate nucleus GABA receptors in essential tremor. Brain 135:105–116. https://doi.org/10.1093/brain/awr301
40. Poewe W, Stankovic I, Halliday G, Meissner WG, Wenning GK, Pellecchia MT et al (2022) Multiple system atrophy. Nat Rev Dis Primers 8:56. https://doi.org/10.1038/s41572-022-00382-6
41. Sakai K, Ishida C, Morinaga A, Takahashi K, Yamada M (2015) Case study: somatic sprouts and halo-like amorphous materials of the purkinje cells in Huntington's disease. Cerebellum 14:707–710. https://doi.org/10.1007/s12311-015-0678-4
42. Seidel K, Siswanto S, Brunt ER, den Dunnen W, Korf HW, Rub U (2012) Brain pathology of spinocerebellar ataxias. Acta Neuropathol 124:1–21. https://doi.org/10.1007/s00401-012-1000-x
43. Tanabe K, Kani S, Shimizu T, Bae YK, Abe T, Hibi M (2010) Atypical protein kinase C regulates primary dendrite specification of cerebellar Purkinje cells by localizing Golgi apparatus. J Neurosci 30:16983–16992. https://doi.org/10.1523/JNEUROSCI.3352-10.2010
44. Yang Q, Hashizume Y, Yoshida M, Wang Y, Goto Y, Mitsuma N et al (2000) Morphological Purkinje cell changes in spinocerebellar ataxia type 6. Acta Neuropathol 100:371–376. https://doi.org/10.1007/s004010000201
45. Yoshida K, Asakawa M, Suzuki-Kouyama E, Tabata K, Shintaku M, Ikeda S et al (2014) Distinctive features of degenerating Purkinje cells in spinocerebellar ataxia type 31. Neuropathology 34:261–267. https://doi.org/10.1111/neup.12090
46. Yu M, Ma K, Faust PL, Honig LS, Cortes E, Vonsattel JP et al (2012) Increased number of Purkinje cell dendritic swellings in essential tremor. Eur J Neurol 19:625–630. https://doi.org/10.1111/j.1468-1331.2011.03598.x

**Publisher's Note** Springer Nature remains neutral with regard to jurisdictional claims in published maps and institutional affiliations.

Springer Nature or its licensor (e.g. a society or other partner) holds exclusive rights to this article under a publishing agreement with the author(s) or other rightsholder(s); author self-archiving of the accepted manuscript version of this article is solely governed by the terms of such publishing agreement and applicable law.